Plasmablast-derived antibody response to acute SARS-CoV-2 infection in humans

Kuan-Ying A. Huang[1,2†], *Tiong Kit Tan*[3#], *Ting-Hua Chen*[4], *Chung-Guei Huang*[1,5], *Ruth Harvey*[6], *Saira Hussain*[6], *Cheng-Pin Chen*[7], *Adam Harding*[8], *Javier Gilbert-Jaramillo*[8], *Xu Liu*[8], *Michael Knight*[8], *Lisa Schimanski*[3,9], *Shin-Ru Shih*[1,5], *Yi-Chun Lin*[10], *Chien-Yu Cheng*[7], *Shu-Hsing Cheng*[10], *Yhu-Chering Huang*[2], *Tzou-Yien Lin*[2], *Jia-Tsrong Jan*[4], *Che Ma*[4], *William James*[8], *Rodney S. Daniels*[6], *John W. McCauley*[6], *Pramila Rijal*[3,9#], *Alain R. Townsend*[3,9†]

[1] Research Center for Emerging Viral Infections, College of Medicine, Chang Gung University, Taoyuan, Taiwan

[2] Division of Pediatric Infectious Diseases, Department of Pediatrics, Chang Gung Memorial Hospital, Taoyuan, Taiwan

[3] MRC Human Immunology Unit, Weatherall Institute of Molecular Medicine, University of Oxford, John Radcliffe Hospital, Oxford, UK

[4] Genomics Research Center, Academia Sinica, Taipei, Taiwan

[5] Department of Laboratory Medicine, Chang Gung Memorial Hospital, Taoyuan, Taiwan

[6] Worldwide Influenza Centre, The Francis Crick Institute, 1 Midland Road, London NW1 1AT, UK

[7] Department of Infectious Diseases, Taoyuan General Hospital, Ministry of Health and Welfare, Taoyuan, and National Yang-Ming University, Taipei, Taiwan

[8] Sir William Dunn School of Pathology, University of Oxford, Oxford, UK

[9] Centre for Translational Immunology, Chinese Academy of Medical Sciences Oxford Institute, University of Oxford, Oxford, UK

[10] Department of Infectious Diseases, Taoyuan General Hospital, Ministry of Health and Welfare, Taoyuan, and Taipei Medical University, Taipei, Taiwan

# Tiong Kit Tan and Pramila Rijal contributed equally.

† Correspondence: Kuan-Ying A. Huang arthur1726@cgmh.org.tw, or Alain R. Townsend alain.townsend@imm.ox.ac.uk

Abstract

Plasmablast responses and derived IgG monoclonal antibodies (MAbs) have been analysed in three COVID-19 patients. An average of 13.7% and 13.0% of plasmablast-derived IgG MAbs were reactive with virus spike glycoprotein or nucleocapsid, respectively. Of thirty-two antibodies specific for the spike glycoprotein, ten recognised the receptor-binding domain (RBD), thirteen were specific for non-RBD epitopes on the S1 subunit, and nine recognised the S2 subunit. A subset of anti-spike antibodies (10 of 32) cross-reacted with other betacoronaviruses tested, five targeted the non-RBD S1, and five targeted the S2 subunit. Of the plasmablast-derived MAbs reacting with nucleocapsid, over half of them (19 of 35) cross-reacted with other betacoronaviruses tested. The cross-reactive plasmablast-derived antibodies harboured extensive somatic mutations, indicative of an expansion of memory B cells upon SARS-CoV-2 infection. We identified 14 of 32 anti-spike MAbs that neutralised SARS-CoV-2 in independent assays at ≤ 133 nM (20 µg/ml) (five of 10 anti-RBD, three of 13 anti-non-RBD S1 subunit, six of nine anti-S2 subunit). Six of 10 anti-RBD MAbs showed evidence of blockade of ACE2 binding to RBD, and five of six of these were neutralising. Non-competing pairs of neutralising antibodies were identified, which offer potential templates for the development of prophylactic and therapeutic agents against SARS-CoV-2.

Introduction

In late 2019, a novel coronavirus emerged and was identified as the cause of a cluster of respiratory infection cases in Wuhan, China. It spread quickly around the world. In March of 2020 a pandemic was declared by the World Health Organization , the virus was formally named as Severe Acute Respiratory Syndrome Coronavirus 2 (SARS-CoV-2) and the resulting disease was named COVID-19. As of 12 August 2020, there have been over 20 million confirmed cases of SARS-CoV-2 infection with 737,417 deaths (World Health Organization, https://covid19.who.int/).

There is no fully effective drug or licenced vaccine for COVID-19. Antibodies neutralise SARS-CoV-2 *in vitro*, offering hope that a vaccine may induce a protective response, and antibodies may be an effective treatment for COVID-19 in clinical practice. Convalescent plasma is being tested in ongoing clinical trials as a therapy for COVID-19 (1, 2), and was previously used in the treatment of SARS (3). The virus spike glycoprotein is a target of neutralising antibodies, which makes it a key candidate for both vaccine development and immunotherapy (4). B cell responses in COVID-19 patients have been detected concomitantly with follicular helper T cell responses from week one after illness onset (5). In SARS patients, B cell responses typically arise first against the nucleocapsid protein then, within four to eight days after symptom onset, antibody responses to spike glycoprotein have been found; neutralising antibody responses begin to develop by week two, and most patients develop neutralising antibodies by week three (6). Two serological studies of COVID-19 patients showed anti-SARS-CoV-2 IgG seroconversion at week three after onset and some cross-reactivity to nucleocapsid of SARS (7, 8).

Antibodies may play a role in protection against SARS-CoV-2 infection. The underlying B-cell response leading to the rapid production of plasmablasts (antibody-secreting cells) that secrete antibodies upon natural SARS-CoV-2 exposure/infection is only beginning to be understood (5). Here, we characterised the infection-induced plasmablast response and the derived IgG anti-SARS-CoV-2 spike glycoprotein and nucleocapsid monoclonal antibodies (MAbs) from adult human patients with laboratory-confirmed COVID-19. The antigenic specificity and breadth of antibodies and the sequence of their variable domains have been characterised in detail. Virus neutralising antibodies were detected that bound epitopes on receptor-binding domain (RBD), non-RBD regions of the S1 polypeptide, and the S2 polypeptide of the spike glycoprotein.

Results

Isolation of anti-spike glycoprotein and anti-nucleocapsid IgG antibodies from circulating plasmablasts

Serum IgG antibodies to the virus spike glycoprotein and the isolated RBD were analysed by indirect enzyme-linked immunosorbent and flow cytometry assays in three patients with laboratory-confirmed COVID-19. The clinical characteristics of the three patients studied are shown in Supplementary Table 1. Antibodies to spike glycoprotein and RBD were detected in all three patients after week 3 of illness onset (Figure 1a). Case A showed a robust response to spike glycoprotein and the isolated RBD by day (D) 22 (D22). Longitudinal sera from case B and C showed lower anti-spike glycoprotein and RBD IgG titres at week 1 or the beginning of week 2 and an elevated titre that peaked at the end of week 2 through week 3 (a peak 50% effective dilution (ED_{50}) titre to RBD 1:1,051 at D18 in case B and 1:588 at D14 in case C). Case B had prolonged fever and developed pneumonia at the end of week 2, which was followed by a robust increase of anti-spike glycoprotein and RBD IgG titres at week 3 (Figure 1a, Supplementary Table 1). By contrast, case C experienced a two-day course of febrile illness and reduction of all symptoms within the first week, followed by anti-spike glycoprotein and RBD IgG titres that peaked earlier at the end of week 2 (Figure 1a, Supplementary Table 1).

An increased frequency of circulating plasmblasts was detected in all three patients (healthy adults baseline less than 1%) (5) (Figure 1b). In case A, a plasmablast response containing a substantial IgG subset was detected at the end of week 2 (D14), followed by a high serological titre at week 3 (D22). Case B had a robust plasmablast response at the end of week 2 (D14) but the IgG plasmablast subset continued to rise,

dominated at week 3 (D18), but then subsided at the beginning of week 4 (D22), which is compatible with high anti-spike glycoprotein and RBD IgG serological titres at week 3. Case C produced a significant early plasmablast response at the end of week 1 (D6), the IgG plasmablast subset dominated at the same time, and both the plasmablast response and its IgG subsets subsided at the end of week 2 (D14).

Circulating plasmablasts were identified and used to generate human IgG monoclonal antibodies (MAbs) from the three patients (Figure 2a). A total of 219 plasmablast-derived IgG MAbs were produced, of which 67 (10 of 50 from case A, 48 of 131 from case B, nine of 38 from case C) were shown to bind spike glycoprotein or nucleocapsid antigens of SARS-CoV-2 by one or more of the following: staining of spike glycoprotein and RBD-expressing cells, ELISA, or immunofluorescence and specific virus neutralisation. Averages of 13.7±6.8% (6.0-18.4%) and 13.0±7.3% (5.3-19.9%) of plasmablast-derived IgG MAbs were reactive with virus spike glycoprotein and nucleocapsid, respectively.

Genetic and phenotypic characteristics of anti-spike glycoprotein antibodies

Among 32 MAbs, 10 bound to the RBD, 13 to non-RBD S1, and the other 9 to the S2 subunit of the SARS-CoV-2 spike glycoprotein (Figure 2a and Table 1). Twenty-four of these MAbs bound to virus antigens as assessed by immunofluorescence of SARS-CoV-2-infected Vero E6 cells (Supplementary Figure 1), suggesting that the majority of anti-spike glycoprotein human antibodies recognise complex conformational epitopes on the virus glycoprotein. Weak binding was observed for a subset (4 of 9) of anti-S2 MAbs with full-length spike glycoprotein ectodomain in the indirect ELISA but bound strongly to the isolated S2 subunit (Figure 2b).

Ten of 32 anti-SARS-CoV-2 spike glycoprotein MAbs cross-reacted with the glycoproteins of other betacoronaviruses, including SARS, MERS or human common cold coronavirus OC43 in ELISA (Table 1), suggesting the presence of conserved epitopes on the spike glycoproteins of betacoronaviruses.

Each of 32 anti-spike glycoprotein MAbs was encoded by a unique set of heavy chain VDJ and light chain VJ rearrangements in the variable domain (Supplementary Table 2). Fourteen of 32 SARS-CoV-2 spike-reactive Mab genes possessed low numbers of somatic mutations resulting in 0 or 1 amino acid substitutions suggesting a *de-novo* B cell response to the SARS-CoV-2 virus in humans. Six of the 32 Mab genes possessed $\geq$ 20 nucleotide mutations, and these cross-reacted on other beta-coronaviruses, including OC43. Of the nine anti-S2 antibodies five cross-reacted on OC43 virus and three of these also cross-reacted on MERS (Table 1). All five cross-reactive anti-S2 antibodies had high rates of somatic mutation (25±5), indicating a memory phenotype, and three of the five were neutralising to a moderate level (half maximal effective concentration, EC_{50}, 36-133.33 nM, Table 1).

The CDR3 length varied among anti-spike glycoprotein antibodies (Supplementary Table 2). No significant differences were found between anti-S2 and anti-S1 or anti-RBD subsets. Among anti-S2 MAbs, a significantly longer heavy chain CDR3 length was found in the cross-reactive group compared to the specific group (Cross-reactive 20±2 versus Specific 12±4, p= 0.02; Figure 2c), indicating that a long CDR3 may play a role in antigen binding, which is also found in several broadly reactive human MAbs against human immunodeficiency virus and influenza virus (9, 10).

Characterisation of anti-RBD antibodies

The binding sites of 10 anti-RBD MAbs were further characterised in detail. Using MDCK-SIAT1 cells transduced to express the RBD and flow cytometry, binding activities of the anti-RBD MAbs were shown to vary with 50% binding concentration from 0.10 to 1.83 µg/ml (see methods; Supplementary Figure 2). The MAbs with strong anti-RBD binding have a relatively long heavy chain CDR3 length (50% binding concentration <0.5 µg/ml versus >0.5 µg/ml, p=0.03; Supplementary Figure 3).

Division of anti-RBD antibodies into cross-inhibiting groups

The ten anti-RBD IgG MAbs were divided into cross-inhibiting groups as described for human MAbs to Ebola (11) by assessing competition of unlabelled antibodies at 10-fold (or greater) excess over a biotin labelled target antibody by ELISA. Included as controls were the VHH72-Fc (12) and H11-H4-Fc (13) nanobodies linked to the hinge and Fc region of human IgG1, and CR3022 human MAb (14) reconstituted as an IgG1 antibody. These three control molecules have characterised binding footprints on the RBD defined by crystal structures (12, 13, 15), as does EY 6A (16). Also included was the protease domain (residues 18-615) of ACE2 linked to the Fc region of human IgG1 (ACE2-Fc dimer).

When optimising the binding assay we found that soluble RBD bound to a standard ELISA plate showed reduced binding to a soluble ACE2-Fc molecule (Supplementary Figure 4) compared to RBD displayed on a mi3 Virus Like Particle (RBD-VLP) (17). Therefore, in competition experiments we used the RBD-VLP molecule bound to the plate to display RBD to antibodies or ACE2-Fc.

The ten antibodies formed four cross-inhibiting clusters (Table 2), represented by antibodies EY 6A (cluster 1, which included CR3022), FI 3A (cluster 2), FD 11A

(cluster 3) and FJ 10B (cluster 4). The strongest inhibitors of ACE2-Fc binding were in clusters 2 and 3 (Tables 1 and 2, Supplementary Figure 5). Neutralising antibodies were detected in clusters 1, 2 and 3, with the strongest antibodies FI 3A and FD 11A being in clusters 2 and 3 (Tables 1 and 2).

ACE2 blockade by anti-RBD antibodies

We compared two assays designed to detect antibody-blocking of the ACE2-RBD interaction (Supplementary Figure 5, Table 1), including an assay that we reported previously (13, 16). In the first assay unlabelled MAbs in at least 10-fold excess were mixed with biotin labelled ACE2-Fc and binding to the RBD, displayed on RBD-VLP bound to an ELISA plate, was detected with Streptavidin-HRP (Supplementary Figure 5a). The definition of the antibody clusters in Table 2 was based on this assay.

We noted that when unlabelled ACE2-Fc was used to compete with labelled MAbs a slightly different pattern was detected: for example, the unlabelled nanobody VHH72-Fc in excess strongly inhibited the binding of labelled ACE2-Fc to RBD, but not *vice-versa*. The structure of VHH72-Fc bound to RBD is known (12) and its footprint on the RBD does not overlap that of ACE2, so inhibition is thought to occur by steric hindrance. The second example is the pair FD 5D and FD 11A in cluster 3. These antibodies showed no inhibition of labelled ACE2-Fc, but the biotinylated versions were strongly competed by unlabelled ACE2-Fc (Table 2).

In the second assay, we employed MDCK-SIAT1 cells overexpressing full-length human ACE2 as a transmembrane protein. Unlabelled antibodies or ACE2-Fc were mixed in excess with biotinylated RBD, and binding of RBD was detected with Streptavidin-HRP in ELISA (Supplementary Figure 5b). The results of this assay mostly mirrored those of the first assay and confirmed that in this orientation cluster 3

antibodies FD 5D and FD 11A competed in excess with soluble RBD for binding to ACE2 (Supplementary Figure 5). In addition, antibodies in cluster 1 showed partial (CR3022) or near complete (EY 6A) competition. These two antibodies are known to bind to the same region of RBD away from the ACE2 binding site, but they influence the binding kinetics of RBD to ACE2, presumably through steric effects (16).

Neutralisation by anti-spike glycoprotein antibodies

The optimum method for detecting neutralisation of SARS-CoV-2 has not been established. For example, different laboratories have obtained varying results for the well-defined monoclonal antibody CR3022 (14, 15, 18). We have therefore compared results from neutralisation assays performed in four independent laboratories: a systematic survey of the thirty two anti-Spike MAbs at the Francis Crick Institute (London), with follow up for a selection of MAbs at the Sir William Dunn School (Oxford), Public Health England (Porton Down) and Chang Gung Memorial Hospital (Taiwan).

The 32 anti-spike glycoprotein MAbs were systematically screened at the Francis Crick Institute by plaque reduction neutralisation (PRNT) assay for neutralisation of wild type SARS-CoV-2 virus (see methods; summarised in Table 1). A total of 14 neutralising antibodies distributed between different regions of the spike glycoprotein were identified: three of 13 to S1 (non-RBD), six of nine to S2, five of 10 to RBD. The EC_{50} concentrations, as a measure of potency, ranged from 0.05 nM to ~133.33 nM (8 ng/ml - ~20 µg/ml). Corroboration for a selection of these antibodies was then sought.

Neutralisation was corroborated by a microneutralisation test at Oxford (see methods), that measured a reduction in fluorescent focus-forming units, summarised

in Table 1 and Figure 3. EW 9C and EY 6A inhibited wild-type viruses by PRNT at PHE Porton Down (see methods, Supplementary Figure 6). MAbs were also screened by a PCR-based neutralisation assay at Chang Gung Memorial Hospital (Taiwan) (see methods): inhibition of virus replication was measured by quantitative PCR in the supernatant bathing the infected cells. This assay confirmed that at least five anti-spike glycoprotein antibodies (EW 9C, S2; EY 6A, RBD; FD 5D, RBD; FD 11A, RBD; FI 3A, RBD), as crude culture supernatants from transfected ExpiCHO cells, reduced the virus signal from ~56- to ~10,085-fold (Supplementary Figure 7).

Neutralising antibodies to RBD and relationship to ACE2 blockade

Five neutralising MAbs target the RBD and all of these partially or completely blocked the interaction between RBD and ACE2 in one or the other type of assay (Tables 1 and 2, Supplementary Figure 5). The most potent neutralising antibodies were ACE2 blockers (FI 3A in cluster 2, and FD 11A in cluster 3), and bound independently of each other to the RBD. MAb EY 6A has been shown to alter the binding kinetics of the interaction without full inhibition (16) and it had a moderate effect on ACE2 binding here in the assay where ACE2 was expressed at the cell surface. These three MAbs bound independently of each other indicating the existence of at least three neutralisation-sensitive epitopes within the RBD. All five neutralising MAbs to the RBD (EY 6A, FI 3A, FI 1C, FD 11A, FD 5A) had V gene sequences close to germline (Supplementary Table 2).

Neutralising antibodies to S2

Six of nine MAbs specific for S2 showed moderate neutralisation in the PRNT assay (Table 1). The antibodies FB 1E, FJ 4E and EW 9C, are moderately neutralising (EC_{50} 36-133.33 nM), cross-react on the spike glycoprotein from the common cold

betacoronavirus OC43, and show sequence characteristics of memory cells with high numbers of somatic mutations. This indicates that memory B cells, likely primed by an endemic or epidemic betacoronavirus related to OC43, can give rise to antibodies that neutralise SARS-CoV-2, albeit modestly. The other three neutralising antibodies specific for S2, FD 10A, FG 7A and FM 1A were close to germline in sequence (Supplementary Table 2) and did not cross-react strongly with other betacoronaviruses (Table 1). FD 10A exhibits the most potent neutralising activity in the PRNT assay and completely inhibits SARS-CoV-2-induced cytopathic effect (see methods) at 8.33 nM.

Neutralising antibodies to non-RBD S1

Thirteen MAbs were defined that bound the S1 region and three, close to germline in sequence, were neutralising. FJ 1C showed strong neutralisation (EC_{50} 55.5 nM), whilst FD 11E (EC_{50} 70 nM) and FD 1E (EC_{50} 110 nM) were moderately neutralising (Table 1). We investigated the specificity of these antibodies using flow cytometry with MDCK-SIAT1 cells expressing the N-terminal domain (NTD) of spike glycoprotein linked to the transmembrane and cytoplasmic region of influenza haemagglutinin (see methods). FJ 1C (neutralising) and FD 7C bound strongly to this NTD construct defining them as NTD specific (Table 1, Supplementary Figure 8).

In Table 1 we have summarised all of the results from the Francis Crick institute and the Sir William Dunn School. It will be noted that not all of the results agree, particularly for MAbs directed at epitopes other than the RBD. The results in the two laboratories were reproducible.

Characterisation of anti-nucleocapsid antibodies

A set of 35 anti-SARS-CoV-2 nucleocapsid MAbs were derived from circulating plasmablasts in the naturally infected subjects (Table 3, Supplementary Figure 9); 19 of these strongly cross-react with at least one of the betacoronaviruses tested, 17 with SARS CoV, 14 with OC43 virus, and 13 with MERS CoV in ELISA. This suggested extensive cross-reactivity of the antibody response to epitopes in nucleocapsids of betacoronaviruses following natural infection with SARS-CoV-2.

The 35 MAbs were evolved from 33 clonal groups defined by their heavy chain VDJ and light chain VJ rearrangements (Supplementary Table 3). Those cross-reactive with other betacoronaviruses carried considerably more amino acid substitutions than SARS-CoV-1-specific MAbs in their variable domains (CR heavy 22±15 versus specific heavy 9±11, p=0.008; Figure 2d), supporting the interpretation that approximately 50% of the anti-nucleocapsid antibody response in these three patients was derived from memory B cells, presumably primed by betacoronaviruses endemic to humans and related to OC43.

Antibodies EW 4C, EY 2A and EY 3B bound to paraformaldehyde-fixed and Triton X-100-permeabilised SARS-CoV-2 infected cells by immunofluorescence. These antibodies were screened for binding to fixed and permeabilised infected cells for use in scoring wells in microneutralisation assays. Antibody EY 2A performed well for this purpose.

Discussion

Plasmablast responses

We detected a robust and rapid plasmablast response encoding diverse anti-spike glycoprotein and anti-nucleocapsid antibody populations within 3 weeks of onset of illness in COVID-19 patients. The concomitant serologic response occurred as early as the first week after illness onset, with gradually increasing levels of SARS-CoV-2 spike glycoprotein- and RBD-binding IgG antibodies from the second to third week after symptom onset. The kinetics of plasmablast and virus-specific serologic responses was observed to vary between subjects. Consecutive samples from donor B showed a highly expanded plasmablast subset at the time of progression into pneumonia, followed by class-switching to an IgG-predominant plasmablast response until week three of illness. On the other hand, donor C presented with mild symptoms and produced an early plasmablast response with class-switching at the end of first week of symptom onset. Thevarajan et al demonstrated a similar kinetic of B cell response in a mild COVID-19 case, in whom the peripheral plasmablast response and the SARS-CoV-2-binding IgG antibodies peaked at day eight, soon after the disappearance of fever (5). An early class-switching phenotype of the humoral response was also noted within the first week of onset in paediatric patients who mainly experienced mild illness after SARS-CoV-2 infection, although the immunological basis for this phenotype is unclear (19). Both peak plasmablast frequency and serologic titre for spike glycoprotein were higher in donor B, who presented with severe symptoms, than in donor C. Similar observations on the serologic titre and clinical severity have been reported by others (7, 20).

Cross-reactivity and somatic hypermutation

In this study, a substantial subset of plasmablast-derived anti-S2 (five of nine, 56%) and anti-nucleocapsid antibodies (14 of 35, 40%) cross-reacted with human betacoronavirus OC43. Cross-reactivity among betacoronaviruses has also been reported in polyclonal sera (21, 22). Human coronavirus OC43, discovered in the 1960s, is one of the major betacoronaviruses that cause common colds in the community (23, 24), and severe respiratory infections in elderly and immunocompromised individuals (22, 25). Epidemiologic surveys reveal that OC43 infection can occur in early childhood, and that OC43 seropositivity reaches nearly 90% in adults (26, 27). The S2 component of SARS-CoV-2 spike glycoprotein shares 43~89% amino acid identity with SARS, MERS and OC43, and, similarly, the amino acid sequence of SARS-CoV-2 nucleocapsid protein of is 34~90% homologous to those of other betacoronaviruses (Supplementary Figures 10 and 11), suggesting the presence of conserved epitopes on these antigens.

The presence of pre-existing immune memory to betacoronavirus that cross-react with SARS-CoV-2 is supported by the accumulation of somatic mutations in the genes encoding cross-reactive antibodies isolated from COVID-19 patients (Figures 2c and 2d, Supplementary Tables 2 and 3). This situation is reminiscent of re-exposure to immunogenic epitopes shared by closely related viruses leading to induction of broadly cross-reactive antibodies in patients infected with influenza, dengue or Zika viruses (28-30).

Our results have significance for serologic tests employing the N and S2 antigens of SARS-CoV-2. Serologic surveys, some of which are based on these antigens, with sera from donors infected with SARS-COV-2 during the spring and summer months have shown very high specificity (as judged by comparing convalescent sera from

343 COVID-19 patients versus sera collected in the pre-COVID-19
344 period)(www.gov.uk/government/publications/covid-19-laboratory-evaluations-of-
345 serological-assays). However, if many individuals have memory B cells to S2 and N
346 antigens of circulating betacoronaviruses that cross-react with SARS-CoV-2,
347 concurrent winter infections with these viruses might erode the specificity of
348 serologic tests for SARS-CoV-2 based on these two antigens. Cross-reactivity of
349 antibodies targeting the RBD is much lower, so using this antigen is more likely to
350 give a true indication of SARS-CoV-2 specificity.

351 ***Neutralising antibodies***

352 The 32 MAbs that bound to the spike glycoprotein were systematically tested for
353 neutralisation in two laboratories (summarised in Table 1). Results established that
354 neutralising epitopes were present on the RBD, S1-NTD, S1-non NTD/RBD, and S2
355 regions of the spike glycoprotein. The range of neutralisation EC_{50} titres against live
356 SARS-CoV-2 reported in the literature for human and murine monoclonal antibodies
357 span at least three orders of magnitude, from ng/ml to µg/ml (31, 32). Our results
358 reflect this range. The relationship between EC_{50} titre in neutralisation assays and
359 therapeutic potential is not established, although antibodies to the RBD with EC_{50} in
360 the nanogram range have shown therapeutic activity in small animal models (33-35).
361 The majority of the most strongly neutralising antibodies were close to germline in
362 sequence, showing that full affinity maturation is not required in order to achieve
363 SARS-CoV-2 virus neutralisation. We made a similar observation for antibodies
364 induced by an Ebola vaccine (11), and this has been observed in other collections of
365 Monoclonal antibodies to SARS-CoV-2 (4,32-39).

The RBDs of SARS and SARS-CoV-2 are known to contain neutralising epitopes (16, 31-42), and vaccines based on the RBD of SARS and SARS-CoV-2 induce strong neutralising antibodies that are protective in animal models (43-45). There is a tendency for the most potent neutralising antibodies to be those that block the binding of the RBD to its receptor ACE2 (31-42, 46-48). Occasional antibodies that do not occupy the ACE2 footprint and fail to block ACE2 binding, can be almost as powerful (40), perhaps through triggering a conformational change in the spike glycoprotein that renders it non-functional (4, 16).

We describe ten MAbs targeting the RBD that can be arranged into four cross-inhibiting clusters (Table 2). Three of these Mab clusters (represented by EY 6A, FI 3A and FD 11A) demonstrate neutralisation of SARS-CoV-2 to some level, while those in the fourth (represented by FM 7B) did not neutralise. This suggests that three neutralising antibodies may be able to bind to the RBD simultaneously. The most potent neutralising MAbs fall in two clusters and interfere strongly with ACE2 binding, something which may be exploited therapeutically. For instance, antibodies FI 3A in cluster 2 (EC_{50} 8.67 nM) and FD 11A in cluster 3 (EC_{50} 0.05 nM) could be combined to limit possible selection of neutralisation-resistant variants. This principle has been demonstrated recently (35, 37, 49).

Neutralisation by human MAbs to the S1-NTD of SARS-CoV-2 has been described (34, 50), but their mechanism of action is not known. The range of neutralising EC_{50} titres (0.09-51.1 nM) was overlapping with those targeting the RBD, similar to our NTD-specific antibody FJ 1C. Cocktails of antibodies that include a representative to the NTD would further reduce the likelihood of selecting neutralisation-resistant viruses. A second strong binder to the NTD, FD 7C, was not strongly neutralising.

Structural comparisons of these two antibodies bound to spike glycoprotein may provide insight into the neutralising action of FJ 1C.

We detected a subset of six MAbs to the S2 region of the spike glycoprotein that neutralised moderately (EC_{50} 36-133 nM). Three of these were clearly derived from a memory population; showing significant accumulation of somatic mutations in the MAb encoding genes and cross-reactivity for the OC43 common cold virus spike glycoprotein (Figure 2c). Further investigation is required to ascertain whether such antibodies, that may be weak- or non-neutralising and cross-reactive with common cold viruses, are beneficial or detrimental with respect to COVID-19 disease.

In summary, COVID-19 patients developed strong anti-SARS-CoV-2 spike glycoprotein and nucleocapsid plasmablast responses. A panel of 32 IgG MAbs targeted a diverse spectrum of epitopes on the RBD, S1-NTD, non-NTD/RBD S1 and S2 regions of the spike glycoprotein, of which 14 neutralised wild type virus with EC_{50}s in the range 0.05 to ~133 nM. Neutralising activities of the majority of anti-RBD MAbs were linked to ACE2-binding blockade, and non-competing pairs of such MAbs, perhaps combined with a neutralising MAb to the NTD, offer potential formulations for the development of prophylactic and therapeutic agents against SARS-CoV-2. Antibody responses to nucleocapsid and the S2 component of spike glycoprotein confirm marked cross-reactivity with a common cold virus.

Materials and Methods

Study design

This study was designed to isolate SARS-CoV-2 antigen-specific MAbs from peripheral plasmablasts of humans infected with SARS-CoV-2 and to characterise the antigenic specificity and phenotypic activities of the MAbs. Diagnosis of SARS-CoV-2 infection was based on positive real-time reverse transcriptase polymerase chain reaction results of respiratory samples. The study protocol and informed consent were approved by the ethics committee at the Chang Gung Medical Foundation and the Taoyuan General Hospital, Ministry of Health and Welfare. Each patient provided signed informed consent. The study and all associated methods were carried out in accordance with the approved protocol, the Declaration of Helsinki and Good Clinical Practice guidelines.

Staining and sorting of plasmablasts

Freshly separated peripheral blood mononuclear cells (PBMCs) or thawed PBMCs were stained with fluorescent-labelled antibodies to cell surface markers purchased from BD Biosciences, USA; Pacific blue anti-CD3 (clone UCHT1, Cat. No. 558117, BD), Fluorescein isothiocyanate anti-CD19 (clone HIB19, Cat. No. 555412, BD), Phycoerythrin-Cy7 anti-CD27 (clone M-T271, Cat. No. 560609, BD), Allophycocyanin-H7 anti-CD20 (clone L27, Cat. No. 641396, BD), Phycoerythrin-Cy5 anti-CD38 (clone HIT2, Cat. No. 555461, BD) and Phycoerythrin anti-human IgG (clone G18-145, Cat. No. 555787, BD). The $CD3^{neg}CD19^{pos}CD20^{neg}CD27^{hi}CD38^{hi}IgG^{pos}$ plasmablasts were gated and isolated in chamber as single cells as previously described (51).

Production of human IgG 1 monoclonal antibodies

Sorted single cells were used to produce human IgG MAbs as previously described (51). Briefly, the variable region genes from each single cell were amplified in a reverse transcriptase polymerase chain reaction (RT-PCR: QIAGEN, Germany) using a cocktail of sense primers specific for the leader region and antisense primers to the Cγ constant region for heavy chain and Cκ and Cλ for light chain. The RT-PCR products were amplified in separate polymerase chain reactions for the individual heavy and light chain gene families using nested primers to incorporate restriction sites at the ends of the variable gene as previously described (51). These variable genes were then cloned into expression vectors for the heavy and light chains. Plasmids were transfected into the HEK293T cell line for expression of recombinant full-length human IgG MAbs in serum-free transfection medium. A selected panel of MAbs were further expanded and purified.

To determine the individual gene segments employed by VDJ and VJ rearrangements and the number of nucleotide mutations and amino acid replacements, the variable domain sequences were aligned with germline gene segments using the international ImMunoGeneTics (IMGT) alignment tool (http://www.imgt.org/IMGT_vquest/input).

Enzyme-linked immunosorbent assay (ELISA)

ELISA plates (Corning® 96-well Clear Polystyrene High Bind Stripwell™ Microplate, USA) were coated with 8 µg/ml SARS-CoV-2 antigens (spike glycoprotein extracellular or receptor-binding domains, or nucleocapsid: Sino Biological, China) or SARS antigen (spike glycoprotein S1 subunit: Sino Biological, China) or Middle East Respiratory Syndrome coronavirus (MERS) antigen (spike glycoprotein extracellular domain: Sino Biological, China) or human coronavirus

OC43 antigen (spike glycoprotein extracellular domain: Sino Biological, China) at 4°C overnight. Plates were washed with phosphate-buffered saline containing 0.05% Tween-20 and blocked with 3% bovine serum albumin (BSA) at room temperature for 1 hour on a shaker. Serial dilutions of MAb-containing cell culture supernatant or purified MAb were added and plates were incubated at 37°C for 1 hour. Plates were washed and incubated with horseradish peroxidase-conjugated rabbit anti-human IgG secondary antibody (Rockland Immunochemicals, USA). Plates were washed and developed with TMB substrate reagent (BD Biosciences, USA). Reactions were stopped with 0.5M hydrochloric acid and absorbances was measured at 450nm on a microplate reader. Non-transfected cell culture supernatant, anti-influenza H3 human IgG MAb BS 1A (in house), anti-SARS spike glycoprotein MAb CR3022 and convalescent serum were used as controls for each experiment. Reaction yielding an absorbance value above three times the mean absorbance of the negative control BS 1A were considered positive.

Flow-cytometry based binding assay

MDCK-Spike cells were produced by stably transfecting parental MDCK-SIAT1 cells with cDNA expressing full-length SARS-CoV-2 spike glycoprotein. MDCK-RBD cells were produced by, stably transducing MDCK-SIAT1 cells with a Lentiviral vector encoding a cDNA expressing RBD amino acids 340-538 (NITN.GPKK underlined) fused via a short linker to the transmembrane domain of haemagglutinin H7 (A/Hong Kong/125/2017) (EPI977395) at the C-terminus for surface expression (sequence:

MNTQILVFALIAIIPTNA/DKIGSGSNITNLCPFGEVFNATRFASVYAWNRKRISN
CVADYSVLYNSASFSTFKCYGVSPTKLNDLCFTNVYADSFVIRGDEVRQIAPG
QTGKIADYNYKLPDDFTGCVIAWNSNNLDSKVGGNYNYLYRLFRKSNLKPFE

RDISTEIYQAGSTPCNGVEGFNCYFPLQSYGFQPTNGVGYQPYRVVVLSFELL HAPATVCGPKKTGSGGSGKLSSGYKDVILWFSFGASCFILLAIVMGLVFICVKN GNMRCTICI*). MDCK-NTD cells were produced by stably transfecting parental MDCK-SIAT1 cells with cDNA expressing SARS-CoV-2 NTD.

Both MDCK-Spike and MDCK-RBD cells were then FACS sorted for highly expressing cells using the CR3022 antibody. MDCK-Spike or MDCK-RBD cells were prepared and resuspended. Cells were probed with purified MAbs in 3% BSA. Bound primary antibodies were detected with FITC-conjugated anti-IgG secondary. The binding activities were analyzed by BD FACSCanto™ II flow cytometer (BD Biosciences, USA).

Immunofluorescence assay

Under biosafety level 3 (BSL-3) conditions, Vero E6 cells were infected with 100 $TCID_{50}$ (median tissue culture infectious dose) SARS-CoV-2 (hCoV-19/Taiwan/CGMH-CGU-01/2020, EPI_ISL_411915). Infected cells were placed on coverslips and, and fixed with acetone at room temperature for 10 minutes. After blocking with 1% BSA at room temperature for 1 hour and washing, fixed cells were incubated with MAb-containing cell culture supernatant. The anti-influenza human monoclonal antibody BS 1A, anti-SARS spike glycoprotein MAb CR3022 and convalescent serum were used as antibody controls for each experiment. Following incubation and wash, cells were stained with FITC-conjugated anti-human IgG secondary antibody and Evans blue dye as counterstain. Antibody-bound infected cells demonstrated an apple-green fluorescence against a background of red fluorescing material stained by the Evans Blue counterstain. Images were acquired with original magnification 40x, scale bar 20 μm.

Plaque reduction neutralisation assay (Francis Crick Institute)

Confluent monolayers of Vero E6 cells in 96-well plates were incubated with ~14 plaque forming units (PFU) of SARS CoV-2 (hCoV-19/England/02/2020, EPI_ISL_407073) and antibodies in a 2-fold dilution series (triplicates) for 3 hours at room temperature. Inoculum was then removed, and cells were overlaid with plaque assay overlay. Cells were incubated at 37°C, 5% CO_2 for 24 hours prior to fixation with 4% paraformaldehyde at 4°C for 30 minutes. Fixed cells were then permeabilised with 0.2% Triton-X-100 and stained with a horseradish peroxidase conjugated-antibody against virus protein for 1 hour at room temperature. TMB substrate was then added to visualise virus plaques as described previously for influenza virus (52). Convalescent serum from COVID-19 patients was used as a control.

Fluorescent focus-forming units microneutralisation assay (FMNT) (Oxford)

In brief, this rapid, high-throughput assay determines the concentration of antibody that produces a 50% reduction in infectious focus-forming units of authentic SARS-CoV-2 in Vero cells, as follows. Triplicate serial dilutions of antibody are pre-incubated with a fixed dose of SARS-CoV-2 (Australia/VIC01/2020, GenBank MT007544) (53) in triplicate before incubation with Vero cells. A carboxymethyl cellulose-containing overlay is used to prevent satellite focus formation. Twenty hours post-infection, the monolayers are fixed with paraformaldehyde and stained for N antigen using MAb EY 2A. After development with a peroxidase-conjugated antibody and substrate, foci are enumerated by enzyme-linked immune absorbent spot reader. Data are analysed using four-parameter logistic regression (Hill equation) in GraphPad Prism 8.3.

Plaque reduction neutralisation assay (Porton Down)

SARS-CoV-2 (Australia/VIC01/2020, GenBank MT007544) (52) was diluted to a concentration of 933 PFU/ml (70 PFU/75 µl) and mixed 50:50 in minimal essential medium (MEM) (Life Technologies, California, USA) containing 1% foetal bovine serum (FBS: Life Technologies) and 25 mM HEPES buffer (Sigma, Dorset, UK) with doubling antibody dilutions in a 96-well V bottomed plate. The plate was incubated at 37°C in a humidified incubator for 1 hour, to allow neutralisation to take place, before the virus-antibody mixture was transferred into the wells of a twice Dulbecco's PBS-washed 24-well plate containing confluent monolayers of Vero E6 cells (ECACC 85020206; PHE, UK) that had been cultured in MEM containing 10% (v/v) FBS. Virus was allowed to adsorb onto cells at 37°C for a further hour in a humidified box and then overlaid with MEM containing 1.5% carboxymethylcellulose (Sigma), 4% (v/v) FBS and 25mM HEPES buffer. After 5 days incubation at 37°C in a humidified box, the plates were fixed overnight with 20% formalin/PBS (v/v), washed with tap water and then stained with 0.2% crystal violet solution (Sigma) and plaques were counted. A mid-point probit analysis (written in R programming language for statistical computing and graphics) was used to determine the dilution of antibody required to reduce numbers of SARS-CoV-2 virus plaques by 50% (ND_{50}) compared with the virus-only control ($n = 5$). The script used in R was based on a previously reported source script (54). Antibody dilutions were run in duplicate and an internal positive control for the PRNT assay was also run in duplicate using a sample of heat-inactivated (56°C for 30 minutes) human MERS convalescent serum known to neutralise SARS-CoV-2 (National Institute for Biological Standards and Control, UK).

Quantitative PCR-based neutralisation assay

Neutralisation activity of MAb-containing supernatant was measured using SARS-CoV-2 (hCoV-19/Taiwan/CGMH-CGU-01/2020, EPI_ISL_411915) infected Vero E6 cells. Briefly, Vero E6 cells were pre-seeded in a 96 well plate at a concentration of 10^4 cells per well. The following day, MAb-containing supernatants were mixed with equal volumes of 100 $TCID_{50}$ virus preparation and incubated at 37°C for 1 hour, then mixtures were added to seeded Vero E6 cells and incubated at 37°C for 5 days. Cell, virus and virus back-titration controls were setup for each experiment. At day 5 the culture supernatant was harvested from each well, and virus RNA was extracted and quantified by real-time RT-PCR targeting the E gene of SARS-CoV-2 as previously described. The cycle threshold values of real-time RT-PCR were used as indicators of the copy number of SARS-CoV-2 RNA in samples with lower cycle threshold values corresponding to higher virus copy numbers.

CPE-based neutralisation assay

Vero E6 cells in Dulbecco's Modified Eagle's Medium containing 10% FBS were added into 96-well plates and incubated at 37°C with 5% CO_2 overnight to reach confluence. After washing with virus growth medium (VGM: Dulbecco's Modified Eagle's Medium containing 2% FBS), two-fold serially diluted MAbs in VGM starting at 100 μg/ml were added to each duplicated well. The plates were immediately transferred to a BSL-3 laboratory and 100 $TCID_{50}$ SARS-CoV-2 (hCoV-19/Taiwan/4/2020, EPI_ISL_411927) in VGM was added. The plates were further incubated at 37°C with 5% CO_2 for three days and the cytopathic morphology of the cells was recorded using an ImageXpress Nano Automated Cellular Imaging System.

Competitive binding assays

Competitive binding assays were performed as described previously (11) with slight modifications for epitope mapping of the anti-RBD MAbs. Briefly, 0.5 µg/ml of RBD-VLP were coated on NUNC plates (50 µl per well) overnight at 4ºC, washed and blocked with 300 µl of 5% (w/v) dried skimmed milk in PBS for 1 hour at room temperature prior to the assays. Antibody was biotinylated using EZ-Link Sulfo-NHS-LC-biotin (21237; Life Technologies) and then mixed with competing MAb (in at least 10-fold excess) and transferred to the blocked NUNC plates for 1 hour. A second layer Streptavidin-HRP (S911, Life Technologies) diluted 1:1,600 in PBS/0.1% BSA (37525; Thermo Fisher Scientific) was then added and incubated for another 1 hour. Plates were then washed, and signal was developed by adding POD substrate (11484281001, Roche) for 5 minutes before stopping the reaction with 1 M H_2SO_4. Absorbance (OD_{450}) was measured using a Clariostar plate reader (BMG, Labtech). Mean and 95% confidence interval of 4 replicate measurements were calculated. Competition was measured as: (X-minimum binding/(maximum binding-minimum binding), where X is the binding of the biotinylated MAb in the presence of competing MAb. Minimum binding is the self-blocking of the biotinylated MAb or background binding. Maximum binding is binding of biotinylated MAb in the presence of non-competing MAb (anti-influenza N1 neuraminidase MAb).

ACE2 blocking assays

Two assays were used to determine the blocking of binding of ACE2 to RBD by MAbs. RBD was anchored on the plate in the first assay whereas ACE2 was anchored for the second assay.

In the first ACE2 blocking assay, RBD-VLP (Spycatcher-mi3 VLP-particles conjugated with Spytagged-RBD recombinant protein) (17) was coated on ELISA

plates as described for the competitive binding assay. Recombinant ACE2-Fc (18-615) protein expressed in Expi293F (Life Technologies) cells was chemically biotinylated using EZ-link Sulfo-NHS-Biotin (A39256; Life Technologies) and buffer exchanged to PBS using a Zebaspin desalting column (Thermo Fischer). MAbs were titrated in duplicate or triplicate as half-log serial dilution, 8-point series starting at 1 µM in 30 µl volume with PBS/0.1% BSA buffer. 30 µl of biotinylated ACE2-Fc at approx. 0.2 nM (40 ng/ml) was added to the antibodies. 50 µl of the mixture was transferred to the PBS-washed RBD-VLP coated plates and incubated for 1 hour at room temperature. Secondary Streptavidin-HRP antibody (S911, Life Technologies) diluted to 1:1600 was then added to the PBS-washed plates and incubated for 1 h at room temperature. Plates were then washed four times with PBS and signal was developed by adding POD substrate (11484281001, Roche) for 5 minutes before stopping with 1 M H_2SO_4. OD450 was measured using a Clariostar plate reader (BMG, Labtech). The control antibody (a non-blocking anti-influenza N1 MAb) or ACE2-Fc without antibody used to obtain the maximum signal and wells with PBS/BSA buffer only were used to determine the minimum signal. Graphs were plotted as % binding of biotinylated ACE2 to RBD. Binding % = {(X - Min)/(Max - Min)}*100 where X = measurement of the antibody, Min = buffer only, Max = biotinylated ACE2-Fc alone. 50% inhibitory concentrations of the antibodies against ACE2 was determined using non-linear regression curve fit using GraphPad Prism 8.

The second ACE2 blocking assay was performed as described previously (13, 16). Briefly, MDCK-SIAT1 cells were stably transfected to overexpress codon-optimised human ACE2 cDNA (NM_021804.1) using lentiviral vector and FACS sorted (MDCK-ACE2). Cells (3×10^4 per well) were seeded on a flat-bottomed 96-well plate the day before the assay. RBD-6H (340-538; NITN.GPKK) was chemically

biotinylated using EZ-link Sulfo-NHS-Biotin (A39256; Life Technologies). Serial half-log dilutions (starting at 1 μM) of antibodies and controls were performed in a U-bottomed 96 well plate in 30 μl volume. 30 μl of biotinylated RBD (25 nM) were mixed and 50 μl of the mixture was then transferred to the MDCK-ACE2 cells. After 1 hour a second layer Streptavidin-HRP antibody (S911, Life Technologies) diluted 1:1,600 in PBS/0.1% BSA (37525; Thermo Fisher Scientific) was added and incubated for another 1 hour. Plates were then washed four times with PBS and signal was developed by adding POD substrate (11484281001, Roche) before stopping with 1 M H_2SO_4 after 5 minutes. OD450 was measured using a Clariostar plate reader (BMG, Labtech). The control antibody (a non-blocking anti-influenza N1 antibody) was used to obtain maximum signal and PBS only wells were used to determine background. Graphs were plotted as % binding of biotinylated RBD to ACE2. The 50% inhibitory concentration of the blocking antibody was determined as described above.

References

1. Bloch, E. M. et al. Deployment of convalescent plasma for the prevention and treatment of COVID-19. *J Clin Invest* 130, 2757-2765 (2020).
2. Li, L. et al. Effect of Convalescent Plasma Therapy on Time to Clinical Improvement in Patients With Severe and Life-threatening COVID-19: A Randomized Clinical Trial. *JAMA* e2010044 (2020).
3. Cheng, Y. et al. Use of convalescent plasma therapy in SARS patients in Hong Kong. *Eur J Clin Microbiol Infect Dis* 24, 44-46 (2005).
4. Walls, A. C. et al. Structure, Function, and Antigenicity of the SARS-CoV-2 Spike Glycoprotein. *Cell* 181, 281-292.e6 (2020).
5. Thevarajan, I. et al. Breadth of concomitant immune responses prior to patient recovery: a case report of non-severe COVID-19. *Nat Med* 26, 453-455 (2020).
6. Nie, Y. et al. Neutralizing antibodies in patients with severe acute respiratory syndrome-associated coronavirus infection. *J Infect Dis* 190, 1119-1126 (2004).
7. Long, Q. X. et al. Antibody responses to SARS-CoV-2 in patients with COVID-19. *Nat Med* 26, 845-848 (2020).
8. Lou, B. et al. Serology characteristics of SARS-CoV-2 infection since exposure and post symptom onset. *Eur Respir J* 2000763 (2020).
9. Ekiert, D. C. et al. Cross-neutralization of influenza A viruses mediated by a single antibody loop. *Nature* 489, 526-532 (2012).
10. West, A. P. Jr et al. Structural insights on the role of antibodies in HIV-1 vaccine and therapy. *Cell* 156, 633-648 (2014).
11. Rijal, P. et al. Therapeutic Monoclonal Antibodies for Ebola Virus Infection Derived from Vaccinated Humans. *Cell Rep* 27, 172-186.e7 (2019).

66412. Wrapp, D. et al. Structural Basis for Potent Neutralization of Betacoronaviruses by
665 Single-Domain Camelid Antibodies. *Cell* 181, 1004-1015.e15 (2020).
66613. Huo, J. et al. Neutralizing nanobodies bind SARS-CoV-2 spike RBD and block
667 interaction with ACE2. *Nat Struct Mol Biol* 10.1038/s41594-020-0469-6 (2020).
66814. ter Meulen, J. et al. Human monoclonal antibody combination against SARS
669 coronavirus: synergy and coverage of escape mutants. *PLoS Med* 3, 237 (2006).
67015. Huo, J. et al. Neutralization of SARS-CoV-2 by Destruction of the Prefusion Spike.
671 *Cell Host Microbe* S1931-3128(20)30351-6 (2020).
67216. Zhou, D. et al. Structural basis for the neutralization of SARS-CoV-2 by an antibody
673 from a convalescent patient. *Nat Struct Mol Biol* 10.1038/s41594-020-0480-y (2020).
67417. Bruun, T. U. J., Andersson, A. C., Draper, S. J. & Howarth, M. Engineering a Rugged
675 Nanoscaffold To Enhance Plug-and-Display Vaccination. *ACS Nano* 12, 8855-8866
676 (2018).
67718. Yuan M, et al. A highly conserved cryptic epitope in the receptor binding domains of
678 SARS-CoV-2 and SARS-CoV. *Science* 368, 630-633 (2020).
67919. Zhang, Y. et al. Protective humoral immunity in SARS-CoV-2 infected pediatric
680 patients. *Cell Mol Immunol* 17, 768-770 (2020).
68120. Zhao, J. et al. Antibody responses to SARS-CoV-2 in patients of novel coronavirus
682 disease 2019. *Clin Infect Dis* ciaa344 (2020).
68321. Hicks, J. et al. Serologic cross-reactivity of SARS-CoV-2 with endemic and seasonal
684 Betacoronaviruses. Preprint. *medRxiv* 2020.06.22.20137695 (2020).
68522. Patrick, D. M. et al. An Outbreak of Human Coronavirus OC43 Infection and
686 Serological Cross-reactivity with SARS Coronavirus. *Can J Infect Dis Med Microbiol*
687 17, 330-336 (2006).

68823. McIntosh, K., Dees, J. H., Becker, W. B., Kapikian, A. Z. & Chanock, R. M.
689 Recovery in tracheal organ cultures of novel viruses from patients with respiratory
690 disease. *Proc Natl Acad Sci U S A* 57, 933-940 (1967).
69124. Nickbakhsh, S. et al. Epidemiology of Seasonal Coronaviruses: Establishing the
692 Context for the Emergence of Coronavirus Disease 2019. *J Infect Dis* 222, 17-25
693 (2020).
69425. Morfopoulou, S. et al. Human Coronavirus OC43 Associated with Fatal Encephalitis.
695 *N Engl J Med* 375, 497-498 (2016).
69626. Severance, E. G. et al. Development of a nucleocapsid-based human coronavirus
697 immunoassay and estimates of individuals exposed to coronavirus in a U.S.
698 metropolitan population. *Clin Vaccine Immunol* 15, 1805-1810 (2008).
69927. Dijkman, R. et al. The dominance of human coronavirus OC43 and NL63 infections
700 in infants. *J Clin Virol* 53, 135-139 (2012).
70128. Beltramello, M. et al. The human immune response to Dengue virus is dominated by
702 highly cross-reactive antibodies endowed with neutralizing and enhancing activity.
703 *Cell Host Microbe* 8, 271-283 (2010).
70429. Rogers, T. F. et al. Zika virus activates de novo and cross-reactive memory B cell
705 responses in dengue-experienced donors. *Sci Immunol* 2, eaan6809 (2017).
70630. Wrammert, J. et al. Broadly cross-reactive antibodies dominate the human B cell
707 response against 2009 pandemic H1N1 influenza virus infection. *J Exp Med* 208, 181-
708 193 (2011).
70931. He, Y., Lu, H., Siddiqui, P., Zhou, Y. & Jiang, S. Receptor-binding domain of severe
710 acute respiratory syndrome coronavirus spike protein contains multiple conformation-
711 dependent epitopes that induce highly potent neutralizing antibodies. *J Immunol* 174,
712 4908-4915 (2005).

71332. Robbiani, D. F. et al. Convergent antibody responses to SARS-CoV-2 in convalescent
714 individuals. *Nature* 10.1038/s41586-020-2456-9 (2020).
71533. Cao, Y. et al. Potent Neutralizing Antibodies against SARS-CoV-2 Identified by High-
716 Throughput Single-Cell Sequencing of Convalescent Patients' B Cells. *Cell* 182, 73-
717 84.e16 (2020).
71834. Liu, L. et al. Potent neutralizing antibodies against multiple epitopes on SARS-CoV-2
719 spike. *Nature* 10.1038/s41586-020-2571-7 (2020).
72035. Wu, Y. et al. A noncompeting pair of human neutralizing antibodies block COVID-19
721 virus binding to its receptor ACE2. *Science* 368, 1274-1278 (2020).
72236. Brouwer, P. J. M. et al. Potent neutralizing antibodies from COVID-19 patients define
723 multiple targets of vulnerability. *Science* 369, 643-650 (2020).
72437. Hansen, J. et al. Studies in humanized mice and convalescent humans yield a SARS-
725 CoV-2 antibody cocktail. *Science* eabd0827 (2020).
72638. Rogers, T. F. et al. Isolation of potent SARS-CoV-2 neutralizing antibodies and
727 protection from disease in a small animal model. *Science* eabc7520 (2020).
72839. Ju, B. et al. Human neutralizing antibodies elicited by SARS-CoV-2 infection. *Nature*
729 584, 115-119 (2020).
73040. Pinto, D. et al. Cross-neutralization of SARS-CoV-2 by a human monoclonal SARS-
731 CoV antibody. *Nature* 583, 290-295 (2020).
73241. Wang, C. et al. A human monoclonal antibody blocking SARS-CoV-2 infection. *Nat*
733 *Commun* 11, 2251 (2020).
73442. Chen, X. et al. Human monoclonal antibodies block the binding of SARS-CoV-2
735 spike protein to angiotensin converting enzyme 2 receptor. *Cell Mol Immunol* 17, 647-
736 649 (2020).

73743. Zhu, X., Liu, Q., Du, L., Lu, L. & Jiang, S. Receptor-binding domain as a target for
738 developing SARS vaccines. *J Thorac Dis* 5 Suppl 2, S142-S148 (2013).
73944. Quinlan, B. D. et al. The SARS-CoV-2 receptor-binding domain elicits a potent
740 neutralizing response without antibody-dependent enhancement. *bioRxiv*
741 2020.04.10.036418 (2020).
74245. Yang, J. et al. A vaccine targeting the RBD of the S protein of SARS-CoV-2 induces
743 protective immunity. *Nature* 10.1038/s41586-020-2599-8 (2020).
74446. Shang, J. et al. Structural basis of receptor recognition by SARS-CoV-2. *Nature* 581,
745 221-224 (2020).
74647. Lan, J. et al. Structure of the SARS-CoV-2 spike receptor-binding domain bound to
747 the ACE2 receptor. *Nature* 581, 215-220 (2020).
74848. Wang, Q. et al. Structural and Functional Basis of SARS-CoV-2 Entry by Using
749 Human ACE2. *Cell* 181, 894-904.e9 (2020).
75049. Baum, A. et al. Antibody cocktail to SARS-CoV-2 spike protein prevents rapid
751 mutational escape seen with individual antibodies. *Science* eabd0831 (2020).
75250. Chi, X. et al. A neutralizing human antibody binds to the N-terminal domain of the
753 Spike protein of SARS-CoV-2. *Science* 369, 650-655 (2020).
75451. Huang, K. A. et al. Structure-function analysis of neutralizing antibodies to H7N9
755 influenza from naturally infected humans. *Nat Microbiol* 4, 306-315 (2019).
75652. Lin, Y. et al. Optimisation of a micro-neutralisation assay and its application in
757 antigenic characterisation of influenza viruses. *Influenza Other Respir Viruses* 9, 331-
758 340 (2015).
75953. Caly, L. et al. Isolation and rapid sharing of the 2019 novel coronavirus (SARS-CoV-
760 2) from the first patient diagnosed with COVID-19 in Australia. *Med J Aust* 212, 459-
761 462 (2020).

76254. Johnson, R. M., et al. Acaricide, fungicide and drug interactions in honey bees (Apis

763 mellifera). *PLoS One* 8, e54092 (2013).

Acknowledgements

We acknowledge the BD FACSAria™ cell sorter service provided by the Core Instrument Center of Chang Gung University. Plasmablast sorting, production and characterisation of human MAbs were supported by the Chang Gung Memorial Hospital (BMRPE22). We would like to acknowledge Paul Sopp and Craig Waugh in the flow cytometry facility at the MRC WIMM for providing cell sorting services. The facility is supported by the MRC HIU, MRC MHU (CC_UU_12009); NIHR Oxford BRC; Kay Kendall Leukaemia Fund (KKL1057), John Fell Fund (131/030 and 101/517), the EPA fund (CF182 and CF170) and by the MRC WIMM Strategic Alliance awards G0902418 and MC_UU_12025. Production of antibodies was funded by the Fast Grant Application given to A.R.T., P.R., and T.K.T. P.R., L.S. and A.R.T. are funded by the Chinese Academy of Medical Sciences (CAMS) Innovation Fund for Medical Science (CIFMS), China (grant no. 2018-I2M-2-002). T.K.T. is funded by the EPA Cephalosporin Fund and The Townsend–Jeantet Charitable Trust (charity no. 1011770). The work done at the Crick Worldwide Influenza Centre was supported by the Francis Crick Institute receiving core funding from Cancer Research UK (FC001030), the Medical Research Council (FC001030) and the Wellcome Trust (FC001030). The Oxford work was funded in part through the generous support of philanthropic donors to the University of Oxford’s COVID-19 Research Response Fund.

Contributions

K.-Y.A.H. conceived and designed the study of MAb isolation and characterization. K.-Y.A.H. produced and characterised plasmablast-derived MAbs. A.R.T. conceived

and designed the study of MAb characterization at Oxford. P.R, T.K.T, L.S generated cell lines, expressed proteins and antibodies, and performed experiments. S.H., R.H. R.S.D and J.W.M. designed and performed neutralisation assay at Crick Institute. A. H., J. G-J., X. L., M. K. and W.J. designed and performed neutralisation assay at Oxford. T-H.C., C-G.H., C-P.C., S-R.S, Y-C.L., C-Y.C., S-H.C., Y-C.H., T-Y.L., J-T.J. and C.M helped prepare materials, perform experiments and analyse data. All authors read and approved the manuscript.

Competing interests

K-Y.A.H. has filed a provisional patent application on anti-spike glycoprotein and anti-nucleocapsid antibodies. Other authors declare no competing interest.

Corresponding authors

Correspondence to Kuan-Ying A. Huang or Alain R. Townsend.

Table 1. The antigenic specificity, cross-reactivity and function of 32 anti-SARS-CoV-2 spike antibodies derived from COVID-19 patients.

Antibody	Case	Domain	SARS-CoV-2[a]				Cross-reactivity[a]			PRNT[b]	FMNT[c]	ACE2 Block[d]	
			IFA	Spike	RBD	S2	SARS	MERS	OC43	EC_{50} (nM)	EC_{50} (nM)	RBD Anchored	ACE2 Anchored
RBD-specific													
FD 11A	B	RBD	pos	1.64	1.17	0.13	0.10	0.10	0.12	0.05	3.68	+	+++
FI 3A	B	RBD	pos	1.60	1.12	0.12	0.08	0.08	0.09	8.67	0.51	++++	++++
FI 1C	B	RBD	pos	1.88	1.22	0.16	0.15	0.15	0.18	16.67	2.24	++	+++
FD 5D	B	RBD	pos	1.83	1.19	0.13	0.09	0.10	0.09	133.33	partial	+	+++
EY 6A	A	RBD	pos	1.75	1.18	0.13	1.82	0.12	0.11	133.33	22.50	-ve	++
EZ 7A	B	RBD	pos	1.66	1.12	0.33	2.05	1.00	1.05	-ve	-ve	-ve	-ve
FI 4A	B	RBD	pos	1.68	1.12	0.12	0.08	0.09	0.10	-ve	-ve	+	-ve
FJ 10B	B	RBD	-ve	1.48	1.22	0.13	1.26	0.10	0.14	-ve	-ve	-ve	-ve
FM 7B	C	RBD	pos	1.80	1.27	0.12	2.25	0.09	0.10	-ve	-ve	-ve	-ve
FN 12A	C	RBD	pos	2.24	1.33	0.30	0.36	0.29	0.38	-ve	-ve	-ve	-ve
S1-non-RBD													
FJ 1C	B	NTD	pos	1.61	0.27	0.15	0.23	0.15	0.16	55.50	partial		
FD 11E	B	non-NTD S1	pos	1.45	0.11	0.12	0.11	0.12	0.14	70.00	-ve		
FD 1E	B	non-NTD S1	pos	1.45	0.11	0.13	0.12	0.12	0.14	110.00	-ve		
EW 8B	B	non-NTD S1	-ve	1.61	0.11	0.13	0.11	0.11	0.12	-ve	-ve		
FD 11D	B	NTD	pos	1.42	0.18	0.22	0.42	0.25	0.29	-ve	partial		
FD 11C	B	non-NTD S1	pos	1.20	0.14	0.20	0.11	0.11	0.12	-ve	partial		
FD 7D	B	non-NTD S1	-ve	1.44	0.12	0.14	0.11	0.11	0.12	-ve	-ve		
FD 8B	B	non-NTD S1	-ve	1.10	0.14	0.12	0.08	0.10	0.09	-ve	-ve		
FD 7C	B	NTD	pos	1.90	0.15	0.15	0.13	0.12	0.13	-ve	35.60		
FG 12C	A	non-NTD S1	pos	1.74	0.14	0.11	0.08	0.08	0.10	-ve	-ve		
FN 8C	C	non-NTD S1	-ve	0.54	0.16	0.16	0.11	0.09	0.12	-ve	-ve		
FD 5E	B	non-NTD S1	pos	0.34	0.16	0.16	0.13	0.11	0.11	-ve	-ve		
EW 9B	B	non-NTD S1	-ve	0.22	0.17	0.11	0.09	0.10	0.09	-ve	-ve		
S2-specific													
FD 10A	B	S2	pos	1.78	0.15	1.32	0.22	0.36	0.39	111.13	-ve		
FB 1E*	C	S2	pos	1.40	0.11	1.20	0.12	1.01	2.34	36.00	-ve		
FJ 4E*	B	S2	-ve	0.26	0.18	0.91	0.18	1.08	1.68	75.33	-ve		
EW 9C*	B	S2	pos	1.22	0.18	1.17	0.14	0.26	1.82	133.33	-ve		
FG 7A	A	S2	pos	0.28	0.17	1.05	0.12	0.13	0.16	133.33	-ve		
FM 1A	C	S2	-ve	0.25	0.17	0.88	0.12	0.09	0.14	133.33	-ve		
FB 9D*	C	S2	pos	1.43	0.12	1.27	0.10	1.50	2.13	-ve	-ve		
FD 1D	B	S2	pos	0.40	0.15	1.06	0.16	0.22	0.25	-ve	-ve		
FN 2C*	C	S2	pos	1.77	0.14	1.15	0.09	0.10	2.20	-ve	-ve		
Controls													
CR3022		RBD	pos	1.08	1.31	0.10	2.24	0.11	0.11	42.00		-ve	-ve
BS 1A		Flu H3	-	0.07	0.09	0.11	0.10	0.09	0.11	-ve		-ve	-ve

[a] A sample (10 µg/ml) was considered positive when the measured extinction is at least 3 times the OD value of the negative control in the ELISA. CR3022 is an anti-SARS RBD human MAb and BS-1A is an anti-influenza H3 human MAb. The OD value ≥ 1.00, 0.50-0.99, or ≤ 0.49 is highlighted in deep green, green and light green, respectively.

[b] The PRNT assay was performed with wild type SARS-CoV-2 at Francis Crick Institute (see methods) and the half maximal effective concentration (EC_{50}) was determined using linear regression analysis.

[c] The FMNT assay was performed with wild type SARS-CoV-2 at Oxford (see methods) and the half maximal effective concentration (EC_{50}) was determined using logistic regression model. Partial: MAb neutralises at least ~40% viruses at 100 nM (highest concentration tested).

[d] ACE2 blocking activity of anti-RBD antibody compared to ACE2-Fc (see methods): +, partial; ++, IC_{50} > ACE2-Fc; +++, IC_{50} ~= ACE2-Fc; ++++, IC_{50} < ACE2-Fc.

* Memory phenotype.

811 Abbreviations: IFA, immunofluorescence; RBD, receptor-binding domain; PRNT, plaque reduction neutralisation
812 assay; FMNT, fluorescent focus-forming units microneutralisation test; ACE2, Angiotensin-Converting Enzyme 2.

Table 2. Competitive binding analysis of anti-SARS-CoV-2 RBD antibodies.[a]

Antibody	Vh	Neut[b]	Cluster	FI 4A-Bio	EY 6A-Bio	CR3022-Bio	VHH72-Fc-Bio	ACE2-Fc-Bio	FI 3A-Bio	FI 1C-Bio	H11-H4-Fc-Bio	FN 12A-Bio	FD 5D-Bio	FD 11A-Bio	FJ 10B-Bio	FM 7B-Bio	EZ 7A-Bio
FI 4A	**3-21**	-	**1**	100	13	-3	27	28	2	2	-1	14	-12	-7	13	4	2
EY 6A	**3-30**	+	**1**	103	100	103	108	-13	1	-2	3	4	22	-5	8	0	-3
CR3022*		+	**1**	103	95	100	107	-1	-3	5	0	-6	45	0	15	10	-1
VHH72-Fc*		+	**1**	103	63	50	100	129	-1	8	-6	-5	15	15	13	2	-4
ACE2-Fc*		+		100	-4	-5	60	100	40	31	8	10	85	67	3	6	0
FI 3A	**3-53**	+	**2**	-27	-1	-3	-20	141	100	97	85	194	-3	-19	21	3	-1
FI 1C	**3-11**	+	**2**	-2	2	4	-17	119	76	100	95	223	20	-4	7	5	1
H11-H4-Fc*		+	**2**	-9	-6	-3	-18	143	66	105	100	217	110	-12	7	0	1
FN 12A	**1-69**	-	**3**	-7	-4	0	-1	4	7	29	-5	100	118	71	7	65	-1
FD 5D	**3-33**	+	**3**	0	0	-6	35	10	2	6	-8	38	100	100	91	58	15
FD 11A	**3-48**	+	**3**	-19	-4	-7	21	5	2	-3	-11	28	114	77	-2	3	7
FJ 10B	**5-10**	-	**4**	15	15	8	-2	6	1	24	16	3	86	12	100	94	98
FM 7B	**1-3**	-	**4**	16	14	5	-19	-5	-5	37	32	40	116	6	103	100	99
EZ 7A	**5-51**	-	**4**	0	2	-3	-2	7	4	3	-8	3	16	4	101	63	100
-ve controls																	
EW 8B		-						0					0	0			
EW 9C		+						0					0	0			
Z3B2*		-		0	0	0	0	0	0	0	0	0	0	0	0	0	0

[a] Competitive inhibition:values are shown for percentage inhibition and those with ≥ 75% blocking, 50-74% blocking, and < 50% blocking are highlighted in red, orange and green, respectively.

[b] Neutralisation of antibody against wild type SARS-CoV-2 was analysed in the PRNT assay (+ = positive, - = negative).

* SARS and SARS-CoV-2 cross-reactive anti-RBD MAb CR3022 was included as a positive control. SARS and SARS-CoV-2 cross-reactive anti-RBD nanobodies VHH72 and H11-H4 linked to the hinge and Fc region of human IgG1 were included as positive controls. ACE2-Fc was included as a positive control. Anti-influenza MAb Z3B2 was included as a negative control.

Table 3. The antigenic specificity and cross-reactivity of 35 anti-SARS-CoV-2 nucleocapsid antibodies derived from COVID-19 patients.

Antibody	Case	SARS-CoV-2[a]	Cross-reactivity[a]			Antibody	Case	SARS-CoV-2[a]	Cross-reactivity[a]		
			SARS	MERS	OC43				SARS	MERS	OC43
EY 12B	A	1.23	1.24	1.10	1.24	**EZ 9B**	B	1.28	0.66	0.72	0.91
EY 9C	A	1.42	1.12	1.07	1.39	**FD 9B**	B	1.11	0.66	0.74	0.47
EY 5A	A	1.40	1.30	1.32	1.32	**FD 3E**	B	1.14	0.69	0.75	0.81
EY 12A	A	1.34	1.37	1.39	1.45	**FD 5B**	B	1.06	0.28	0.58	0.42
EY 2A	A	1.28	1.13	0.31	0.33	**EZ 7B**	B	1.01	0.29	0.29	0.33
EY 3B	A	1.22	1.00	0.22	0.26	**EZ 4A**	B	1.03	0.37	0.36	0.45
EY 8A	A	0.65	0.63	0.66	0.57	**FJ 3C**	B	0.98	1.28	1.16	0.86
						FD 4B	B	0.98	0.43	0.44	0.46
EZ 8C	B	1.34	1.11	1.07	1.44	**FD 4E**	B	0.93	0.53	0.63	0.65
EZ 8B	B	1.38	1.28	1.24	1.12	**FD 4C**	B	0.84	0.47	0.59	0.54
FJ 6D	B	1.30	1.30	1.24	1.05	**FD 8C**	B	0.84	0.46	0.47	0.56
EW 1A	B	1.37	1.36	1.31	1.28	**EZ 4C-1**	B	0.60	0.47	0.26	0.33
EW 9A	B	1.45	1.35	1.24	1.23	**EZ 4C-2**	B	0.71	0.59	0.58	0.34
EW 5A	B	1.37	1.12	1.04	1.30	**EW 10C**	B	0.56	0.62	0.57	0.59
EZ 9A	B	1.51	1.28	1.29	1.13	**EZ 11A**	B	0.53	0.46	0.46	0.23
EW 4C	B	1.24	1.23	1.24	1.31						
FD 6D	B	1.73	1.19	0.12	0.21	**FB 9B**	C	1.27	1.28	0.13	0.21
EZ 11C	B	1.46	0.73	0.72	1.16	**FL 9B**	C	0.92	0.60	0.68	0.94
EZ 9C	B	1.53	0.87	0.87	1.27						
Controls											
CR3022		0.07	0.06	0.07	0.17						
BS-1A		0.08	0.07	0.07	0.15						

[a] A sample (10 μg/ml) is considered positive when the measured extinction is at least 3 times the OD_{450} value of the negative control in the ELISA. CR3022 is an anti-SARS RBD human MAb and BS-1A is an anti-influenza H3 human MAb. OD values of ≥ 1.00 or 0.50-0.99 or ≤ 0.49 are highlighted in deep orange, orange and light orange, respectively.

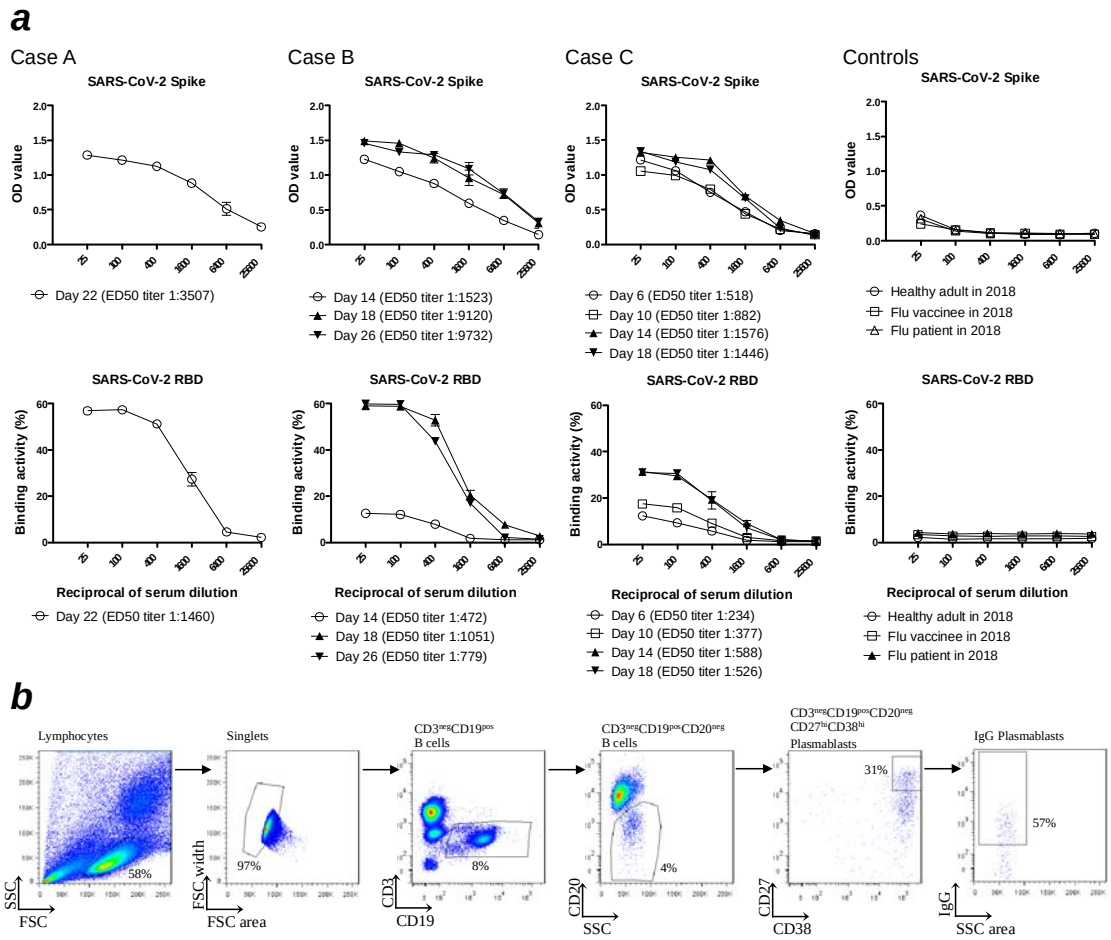

Case	Onset date	Plasmablasts of $CD3^{neg}CD19^{pos}$ B cells (%)	IgG Plasmablasts of B cells(%)	IgG Plasmablasts of Plasmablasts (%)
A	D14	1.99	0.34	16.95
B	D14	37.48	1.67	4.47
	D18	1.13	0.64	56.93
	D22	0.20	0.05	23.33
C	D2	2.56	0.11	4.38
	D6	2.09	0.97	46.39
	D14	0.83	0.09	11.11

Figure 1. The IgG serology and plasmablast response to acute SARS-CoV-2 infection among enrolled patients. (a) The binding activity of post-infection sera IgG with SARS-CoV-2 spike glycoprotein in an ELISA and SARS-CoV-2 RBD assessed by flow cytometry on transfected cells, among enrolled patients. Each

831 experiment was repeated twice. Values are presented as mean ± standard error of the
832 mean. Two sera from healthy adults (one collected at day 28 post 2018-19 influenza
833 vaccination and one collected from an influenza-infected patient 9 days after
834 symptom onset) in 2018 were included as controls. Linear regression was used to
835 determine the 50% end-point dilution (ED_{50}). **(b)** The gating strategy used for
836 peripheral total B cells, plasmablasts and IgG plasmablasts in flow cytometry. The
837 frequency of circulating plasmablasts (percentage of total B cells) among enrolled
838 cases was measured by flow cytometry. Onset date (D = Day).

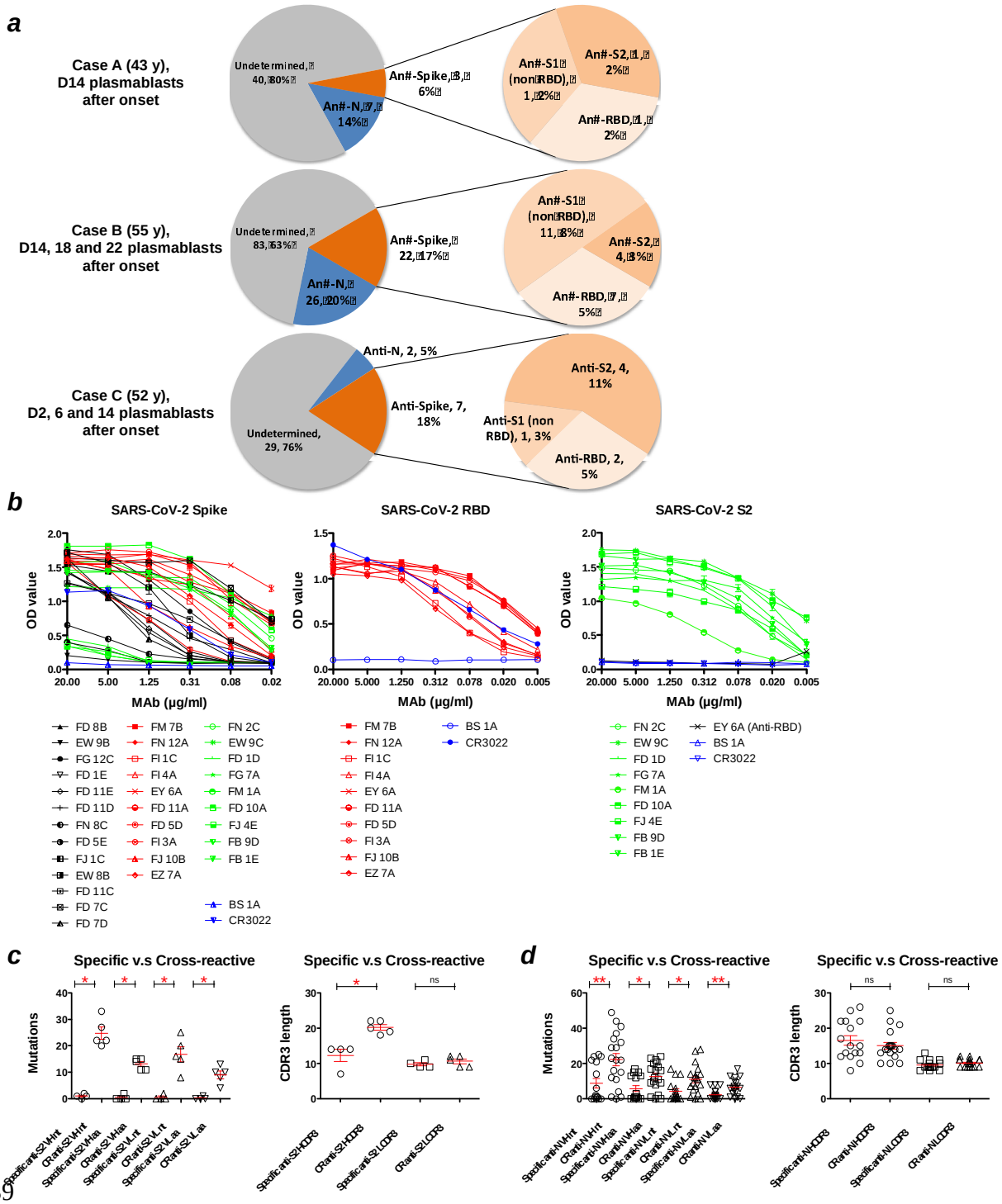

Figure 2. Plasmablast-derived IgG monoclonal antibodies from three COVID-19 patients. (a) A total of 219 IgG monoclonal antibodies were produced from COVID-19 patients (50 from case A, 131 from case B, 38 from case C). An average of

13.7±6.8% and 13.0±7.3% of antibodies were reactive with spike glycoprotein (S) and nucleocapsid (N) antigens of SARS-CoV-2, respectively. The data are presented as specificity, number of antibodies, and the percentage of total antibodies isolated from each patient. **(b)** The binding activity of anti-SARS-CoV-2 MAbs with spike glycoprotein, RBD and the S2 subunit in ELISA. Anti-influenza H3 MAb BS-1A and anti-SARS RBD CR3022 were included as controls. Each experiment was repeated twice. The OD_{450} values are presented as mean ± standard error of the mean. Panels **(c)** and **(d)** show numbers of variable domain mutations in MAb genes and variation in MAb CDR3 lengths among anti-S2 and anti-N MAbs, respectively. Antibodies that strongly cross-react with at least one betacoronavirus (SARS or MERS or OC43) were defined as cross-reactive MAbs. CDR3 length and mutation numbers are presented as mean ± standard error of the mean (anti-S2, specific, n=4 versus cross-reactive, n=5; anti-N, specific, n=16 versus cross-reactive, n=19). The two-tailed Mann-Whitney test was performed to compare the mutations between two groups. * $p < 0.05$, ** $p < 0.01$; D, =Day ; ns, non-significant ; CR, cross-reactive.

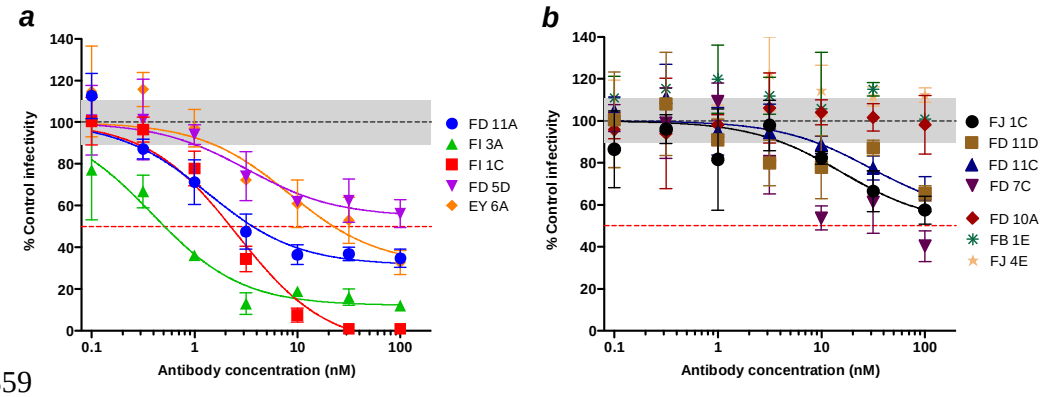

Figure 3. Neutralisation of wild type SARS-CoV-2 by (a) anti-RBD, (b) anti-S1-non-RBD and -S2 monoclonal antibodies. Neutralisation assays were performed on the indicated antibodies according to the fluorescent focus-forming units microneutralisation method (see methods). Data were normalized to control (no antibody) values of foci, and the grey region comprises ± 1 standard deviation the mean control values. Individual points are displayed ± 1 standard deviation of technical, and curves are shown only where the data for a particular antibody fitted the standard dose-response (Hill) equation (n=3).